Simulation of optical gain in AlGaN quantum wells

S.Kölle*§, F. Römer*, G. Cardinali†, A. Schultz†, N. Susilo†, D. Hauer Vidal†,
T. Wernicke†, M. Kneissl†‡, and B. Witzigmann*
*Institute for Optoelectronics, Friedrich-Alexander-Universität Erlangen-Nürnberg, Konrad-Zuse-Str. 3/5, D-91052 Erlangen
†Institute of Solid State Physics, Technische Universität Berlin, Hardenbergstraße 36, D-10623 Berlin
‡Ferdinand-Braun Institute (FBH), Gustav-Kirchhoff-Str. 4, D-12489 Berlin
§Email: sebastian.koelle@fau.de

***Abstract*—Simulations of optical gain in aluminum gallium nitride (AlGaN) quantum wells are extended to the high charge density regime required for achieving gain at 275 nm for UV laser diodes. Coulomb interaction is modeled using the 2nd Born approximation. We demonstrate good agreement with experimental data obtained through optical pumping, and predict gain spectra for electrical pumping.**

***Index Terms*—Simulation, Quantum well lasers, Optoelectronic devices, Aluminum gallium nitride**

I. Introduction

As has recently been demonstrated [1], aluminum gallium nitride (AlGaN) based laser diodes can achieve continuous wave UV-C lasing, although this requires high threshold current densities ($J_{\mathrm{th}} = 4.2\,\mathrm{kA/cm^2}$). Further investigation of this class of UV-C lasers could pave the road for their application in high-resolution manufacturing and imaging. In the following, we examine the impact of quantum well (QW) width and charge density on the gain spectrum.

II. Approach

We solve the semiconductor Bloch equations using bands generated as a self-consistent solution to both the $k{\cdot}p$ method and Poisson equation. Excitonic interactions are incorporated by the second Born approximation [2].

Inhomogeneous broadening (IHB) is calibrated using measurements taken with optical pumping. As practical operation relies on electrical pumping, charge screening is of particular note for this examination. Due to the wurtzite crystal lattice of AlGaN, the strain at QW interfaces causes polarization charges which induce charge separation and thus lower radiative interactions. However, part of these interface charges is screened by an influx of external charges, leading to a reduction of the effective polarization by a factor p_{eff} which is different for both operation modes.

III. Structures

The structures consist of $\mathrm{Al}_x\mathrm{Ga}_{1-x}\mathrm{N}$ layers epitaxially grown on an AlN/sapphire substrate; most notably a 100 nm waveguide with mole fraction $x = 0.63$ in which the QW is embedded. Two different QW designs with width $d_{\mathrm{QW}} = 3\,\mathrm{nm}$ and $d_{\mathrm{QW}} = 9\,\mathrm{nm}$ were investigated, with x chosen for 275 nm emission. The optical confinement factors to convert material gain to modal gain were obtained from simulations as $\Gamma_{3\mathrm{nm}} = 1.3\%$ and $\Gamma_{9\mathrm{nm}} = 5.6\%$.

Funded by the Leibniz Association joint project UVSimTech

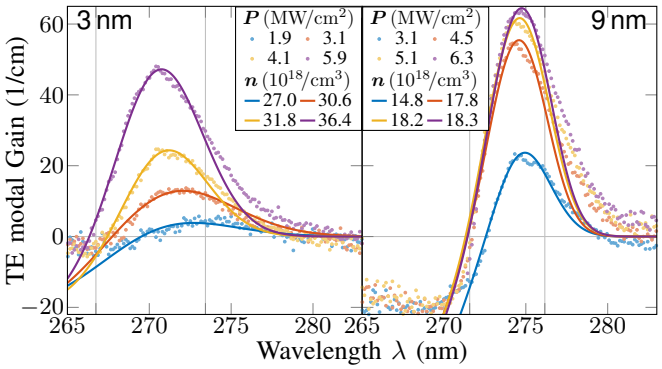

Fig. 1. Measured (dots) vs. simulated (lines) modal gain spectra for optical pumping in 3nm and 9nm QW lasers, at different optical powers P or charge densities $n = p$ respectively. Fitted λ range denoted in grey.

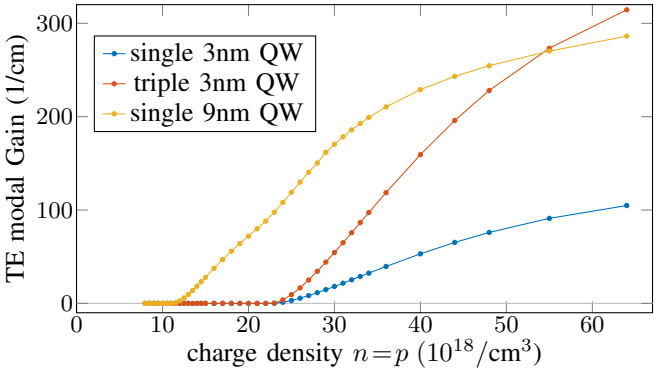

Fig. 2. Peak gain $G_{\max}(n{=}p)$ as a function of charge density, for optical pumping in 3nm and 9nm QW lasers.

IV. Optical pumping

Experimental net gain spectra of the structures were measured using the variable stripe length method (VSLM). The measurements were subject to internal losses of about $10/\mathrm{cm}$ [3] which have been deducted to allow comparison with simulated modal gain spectra (fig. 1).

For optical pumping at the barrier energy, the charges generated by the pump laser outside the active zone screen most of the polarization charges. Both previous and current alignments between experimental and simulated spectra indicate $p_{\mathrm{eff}} \approx 10\%$. We assume that the electron density n and hole density p in the QW are equal.

We limit the fitting range for the IHB parameter σ_{IHB} to the high-energy flank and peak (see fig. 1). With second Born approximation, our gain solver uses postprocessing to apply IHB to gain spectra. As some of the σ_{IHB} exceed the characteristic thermal energy $k_B T$, convolution with a Gaussian cannot reflect redistribution of occupation levels near the transparency frequency. To accommodate for this, the Gaussian broadening algorithm was modified to limit broadening of absorptive transitions across the transparency frequency.

As charge densities increase, occupation levels increase which causes a decrease of IHB as well as a small blueshift of the gain peak by up to $9\,\text{meV}$ for $3\,\text{nm}$ and $5\,\text{meV}$ for $9\,\text{nm}$. When fitting simulations to experiments with low optical power P, they show an IHB of $\sigma_{\text{IHB, 3nm}} = (60 \pm 16)\,\text{meV}$ and $\sigma_{\text{IHB, 9nm}} = (24 \pm 5)\,\text{meV}$ respectively. For higher n, p the IHB quickly converges to $\sigma_{\text{IHB, 3nm}} = (36 \pm 2)\,\text{meV}$ and $\sigma_{\text{IHB, 9nm}} = (19 \pm 4)\,\text{meV}$. The broadened gain spectra, including their corresponding $n = p$, are displayed in fig. 1. We see excellent agreement of measurement and simulation.

Applying the latter set of IHB parameters to an extended series of simulations and only making note of the peak gain $G_{\max}$ for each n, p yields fig. 2.

For the $3\,\text{nm}$ QW, we obtain a transparency density of $n_{\text{th}} = 27 \cdot 10^{18}/\text{cm}^3$ and a differential modal gain of $\partial G = 2.8 \cdot 10^{-18}\,\text{cm}^2$. For the $9\,\text{nm}$ QW, $n_{\text{th}} = 16 \cdot 10^{18}/\text{cm}^3$ and $\partial G = 8.8 \cdot 10^{-18}\,\text{cm}^2$. A combination of three $3\,\text{nm}$ QW would achieve the same differential modal gain, though it wouldn't improve n_{th}.

It should be noted that if we plot $G_{\max}$ over the sheet charge density $n \cdot d_{\text{QW}}$, the differential gain of both QWs is nearly equal at $9.5 \cdot 10^{-12}\,\text{cm}$ and the transparency sheet charge of the narrower QW is actually lower, at $8 \cdot 10^{12}/\text{cm}^2$ versus $14 \cdot 10^{12}/\text{cm}^2$.

V. Electrical pumping

For electrical pumping, we assume $p_{\text{eff}} \approx 50\%$ and $n \approx p$. As such, only p_{eff} is changed between the simulations for optical versus electrical pumping.

The simulated gain spectra for $p_{\text{eff}} = 50\%$ in fig. 3 show the same behaviour as we observed for optical pumping, though with a redshift for lower charge densities as well as a higher transparency density. Both of these effects are explained by the quantum-confined Stark effect due to the distorted potential at low n, p where the polarization charges cannot be compensated with free charges.

It is noteworthy that, had we not included IHB, we would see that the $9\,\text{nm}$ spectrum actually consists of multiple peaks which are smoothed out in practice.

VI. Comparison

As a reference to compare n_{th} and ∂G, neither charge densities (for which the $9\,\text{nm}$ QW would always be preferable) nor sheet charges (which favor the $3\,\text{nm}$ QW) are a representative measure. Instead, we refer to fig. 1 and simulate gain curves with the same charge densities as in that plot. For this selection, we see in fig. 3 that the gain of the $9\,\text{nm}$ QW is notably lower.

Another difference is which transitions contribute to the gain peak. For brevity, let CB1-HH1 denote the transition from conduction band ground state to heavy hole band ground state, with higher indices for excited states. For the $3\,\text{nm}$ QW, CB1-HH1 is dominant with 75-84% contribution in both operation modes.

The $9\,\text{nm}$ QW is wide enough that CB2 is only $43\,\text{meV}$ above CB1. As such, CB2 possesses significant occupation above $n = p = 20 \cdot 10^{18}/\text{cm}^3$. For optical pumping, this means that CB2-HH2 (48%) appears in addition to CB1-HH1 (51%). Finally, electrical pumping of the $9\,\text{nm}$ QW has no true dominant transition, a total of five transitions each contribute anywhere from 11-38%. This is due to the deformed potential breaking the symmetry of eigenstates, thereby allowing classically forbidden transitions.

VII. Conclusion

Our simulations explain the measured gain spectra, which transitions contribute to them, and how charge density, QW width, and pumping method affect gain. Further work will be needed to identify the correct densities n, p for a given current density.

References

[1] Z. Zhang, M. Kushimoto, A. Yoshikawa, K. Aoto, C. Sasaoka, L. J. Schowalter, and H. Amano, "Key temperature-dependent characteristics of AlGaN-based UV-C laser diode and demonstration of room-temperature continuous-wave lasing," *Appl. Phys. Lett.*, vol. 121, no. 22, 11 2022, 222103. [Online]. Available: https://doi.org/10.1063/5.0124480

[2] B. Witzigmann, V. Laino, M. Luisier *et al.*, "Microscopic analysis of optical gain in InGaN/GaN quantum wells," *Appl. Phys. Lett.*, vol. 88, no. 2, 01 2006, 021104. [Online]. Available: https://doi.org/10.1063/1.2164907

[3] M. Martens, C. Kuhn, T. Simoneit, S. Hagedorn, A. Knauer, T. Wernicke, M. Weyers, and M. Kneissl, "The effects of magnesium doping on the modal loss in AlGaN-based deep UV lasers," *Appl. Phys. Lett.*, vol. 110, no. 8, 02 2017, 081103. [Online]. Available: https://doi.org/10.1063/1.4977029

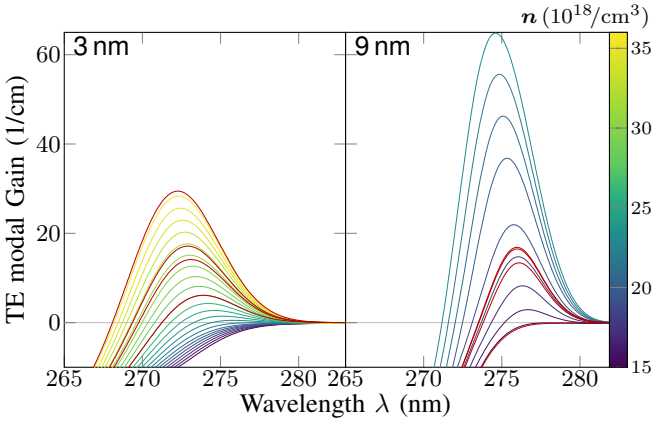

Fig. 3. Simulated gain spectra $G(\lambda)$ for 50% screening in 3nm and 9nm QW lasers. Highlighted curves correspond to densities in fig. 1.